Eruptive dynamics in Plinian silicic eruptions

Preprint, compiled June 3, 2020

Sahand Hajimirza[1*], Helge M. Gonnermann[1], and James E. Gardner[2]

[1]Department of Earth, Environmental and Planetary Sciences, Rice University, Houston, TX, USA
[2]Jackson School of Geosciences, University of Texas at Austin, Austin, TX, USA

Abstract

Magmatic volatiles, of which H_2O tends to be the most abundant, provide the potential energy required for magma explosivity. Explosive eruptions of silica rich magmas produce tephra with exceedingly high bubble number density. Upon ascent to the surface magma decompresses and volatiles become supersaturated, causing bubbles to nucleate with a rate dependent on the degree of supersaturation. A critical dynamical parameter for nucleation, as well as explosive magma fragmentation is the decompression rate. Bubble number density provides a record of magma decompression because of the feedback between decompression, supersaturation, nucleation, and volatile diffusion into nucleated bubbles. Several discrepancies have, however, cast doubt on conventional approach for interpretations of bubble number density. The conventional estimates of decompression rate are unrealistically high. Moreover, inferred pre-eruptive saturation pressures are often too low to overcome the surface energy barrier for homogeneous nucleation. To resolve these discrepancies, we simulate bubble nucleation in eruptions. We demonstrate that bubble number densities and saturation pressures of Plinian silicic eruptions can be reconciled with heterogeneous nucleation facilitated by magnetite nanolites.

1 Introduction

Plinian eruptions are among Earth's most explosive volcanic events and are typically associated with magmas of high silica content [1]. In the past 100 kyr, Plinian silicic eruptions have occurred around the globe, including at volcanoes located in proximity to populated regions (Figure 1a). These eruptions have tremendous destructive power and present extensive risks both locally and globally. The destructive potential of such eruptions derives from the myriad of gas bubbles within the erupting magma. Bubbles contain a highly compressible fluid mixture of exsolved magmatic volatiles, predominantely H_2O [2], and provide the potential energy required for explosive eruptions [3]. Magma explosivity results from fragmentation, thought to depend on the rate at which magma decompresses during ascent [4, 5]. Because eruptive processes are inaccessible to direct observation, understanding explosive volcanism is contingent upon reconstructing governing processes and controlling parameters from indirect observations. The number density of bubbles preserved in erupted pyroclasts is one such observation and is of critical importance in elucidating the dynamical feedbacks between magma decompression, water exsolution, and explosive magma fragmentation.

Bubble nucleation rate and the resultant bubble number density are governed by the feedback between H_2O exsolution and magma decompression. The latter is a consequence of the combined decrease in static pressure, as magma rises toward the surface, and pressure loss from viscous resistance to flow [3]. Consequently, decompression rate depends dynamically on magma discharge rate, conduit dimensions, and magma viscosity. The latter increases as H_2O, initially dissolved within the silicate melt, exsolves into bubbles by diffusion. The efficiency of diffusion, in turn, is rate limited by the number density of bubbles. Slow diffusion kinetics facilitate large supersaturations and therefore higher rates of bubble nucleation. The observed bubble number density in eruptions is thus governed by complex feedbacks between several physical processes. Reconstruction of these processes for a reliable estimation of magma decompression rate requires quantitative models of eruption dynamics, together with bubble nucleation that is calibrated with experimental results.

Bubble number densities preserved in pyroclasts from Plinian silicic eruptions are high and span a narrow range of $10^{15\pm1}$ m^{-3} despite more than 3 wt% variation in pre-eruptive H_2O concentration. Bubbles are thought to form homogeneously within a disordered silicate melt structure because bubbles are exceedingly more abundant than the detected heterogeneities in pyroclasts [6, 7, 8, 9, 10]. Figure 1b compares the observed bubble number densities with experimental results of homogeneous nucleation in rhyolite. The data are presented in terms of potential maximum supersaturation pressure, which is the difference between H_2O saturation and final pressures for experiments, and saturation and atmospheric pressures for eruptions. Experiments suggest that homogeneous nucleation typically initiates at supersaturations of $\approx$110 MPa. Bubble number density increases with supersaturation, and reaches the range of bubble number density observed in eruptions at supersaturations of >150 MPa. Such high pressures, however, are greater than the saturation pressure for most eruptions. Moreover, the conventional estimates of decompression rate, based on homogeneous nucleation, are unrealistically high, $\sim$100 MPa s^{-1}, and are not correlated with magma discharge rate (Figure 1c). In addition, they are substantially greater than decompression rate estimates, which are in the range of $\leq$1 MPa s^{-1}, for independent methods. These results present a quandary that Plinian eruptions are driven by bubbles, but the H_2O saturation pressure and magma decompression rate are often insufficient to nucleate appreciable number of bubbles. The objective of the present work is to resolve some of these discrepancies and thereby advance our ability for quantitative assessment of Plinian volcanic processes and hazards.

*correspondence: sahand@rice.edu

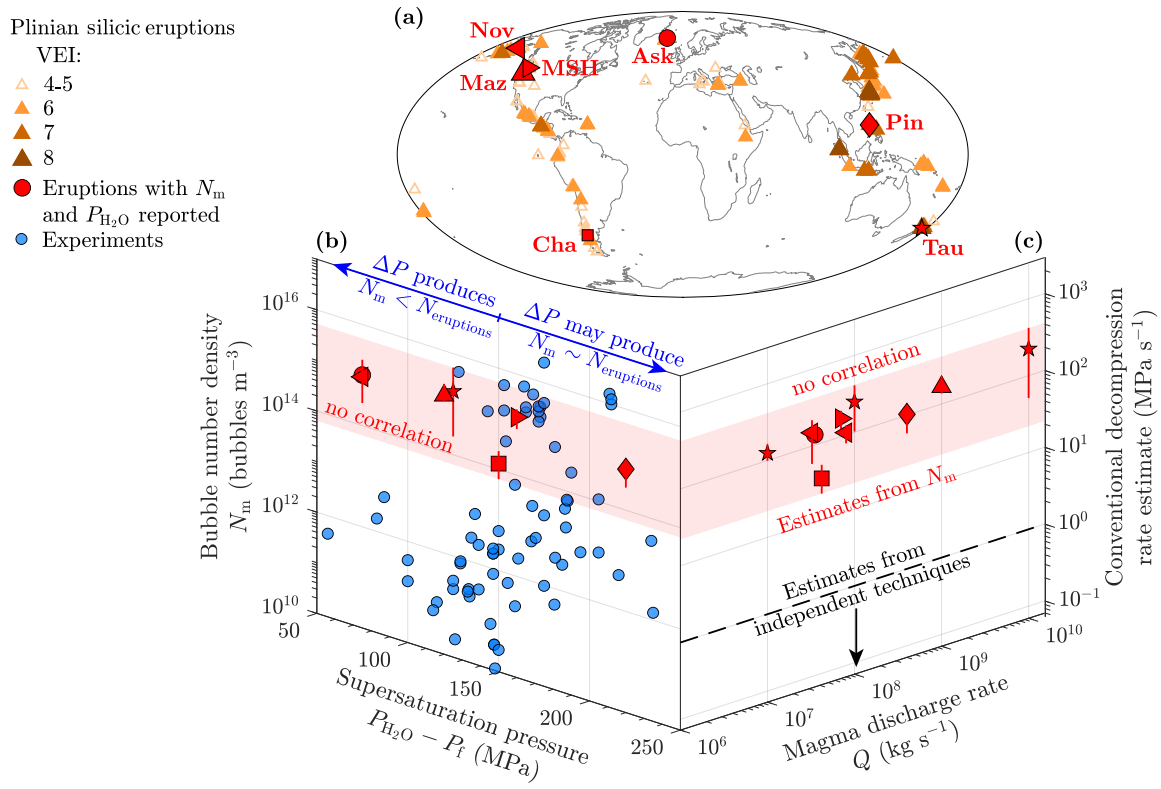

Figure 1: (a) Spatial distribution of Plinian (Volcanic Explosivity Index ≥ 4) silicic eruptions over the past 100 kyr, based on Crosweller et al. [11]. Red symbols are eruptions for which bubble number density and H_2O saturation pressure are known. They are: 1875 Askja (Ask) [8, 12]; 2008 Chaiten (Cha) [7, 13]; 7.7 ka Mount Mazama (Maz) [10, 14], 1980 Mount St. Helens (MSH) [15, 16, 17]; 1912 Novarupta (Nov) [6, 18]; 1991 Pinatubo (Pin) [19, 20]; 1.8 ka Taupo (Tau) [9] eruptions. (b) Bubble number density versus the difference between H_2O saturation and atmospheric pressures for eruptions (red symbols) and the difference between H_2O saturation and final pressures for homogeneous nucleation experiments (blue symbols) [21, 22, 23, 24, 25, 26, 27, 28, 29, 30]. The red shaded area shows the range of bubble number density observed in eruptions. Experiments that are supersaturated for ≥ 150 MPa may fall on the shaded area. (c) The conventional estimates of decompression rate from homogeneous nucleation [31]. Estimated decompression rate for Plinian eruptions is ~100 MPa/s and is not correlated with magma discharge rate.

2 BUBBLE NUCLEATION

When magma decompresses to a pressure lower than the saturation pressure of H_2O, it becomes supersaturated. Supersaturation is a thermodynamic disequilibrium and drives bubble nucleation, defined as formation of H_2O molecules clusters which are stable and can grow into bubbles. According to Classical Nucleation Theory, a cluster is stable if it is larger than a critical size, which is inversely correlated with supersaturation pressure. As a consequence, the rate of formation of stable clusters, known as bubble nuclei, increases with increasing supersaturation. Bubble nuclei are of the order of a few nanometers in size [25, 32] and will grow into micro- to millimeter size bubbles. The energy, W_n, associated with the formation of a bubble nucleus derives from the balance between a reduction of free energy, caused by the clustering of volatile molecules, and an increase in free energy, caused by the formation of a new interface that separates volatiles molecules within the cluster from the surrounding melt. The bubble nucleation rate, in turn, depends exponentially on W_n [32].

To examine the conditions under which bubbles in Plinian pyroclasts may have nucleated, we simulate bubble nucleation and growth during magma decompression (see methods for details on the numerical simulation). We consider H_2O as the dominant volatile phase, because it is the most abundant [2] and it primarily controls the final bubble number density [33]. Our simulations predict nucleation rate during decompression from an initial saturation pressure until magma fragmentation. Dependent parameters are: the pressure inside bubbles and in the surrounding melt, the average concentration of dissolved H_2O in the melt, nucleation rate, bubble number density, and bubble size. We use the model of Hajimirza et al. [25] which have been previously tested against homogeneous bubble nucleation experiments in rhyolite. It has been demonstrated that the model reliably predicts experimental results under a wide range of saturation pressures and decompression rates.

In homogeneous nucleation W_n is large and a high supersaturation pressure is thus required to overcome the surface energy barrier of a nucleus formation [25, 27]. In our simulations, we first examined whether the observed bubble number density in each eruption can be produced by homogeneous nucleation. If

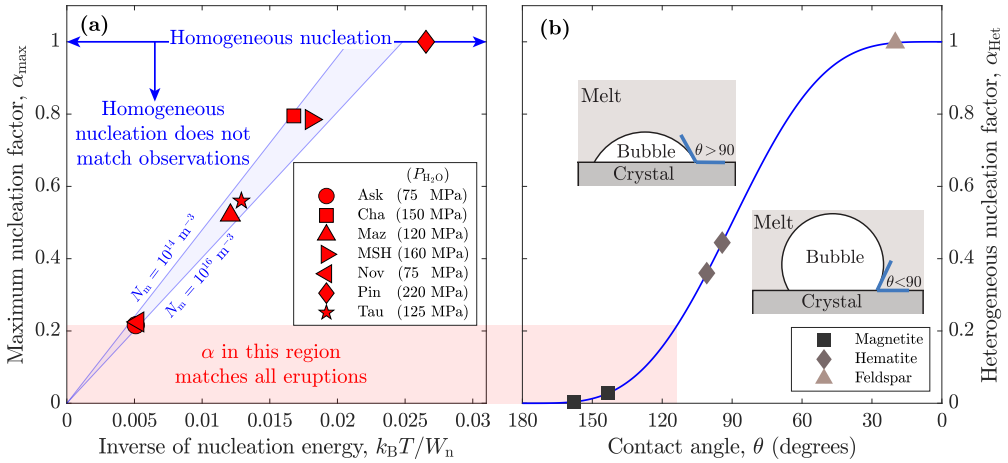

Figure 2: (a) The maximum value of nucleation factor as a function of nucleation energy and observed bubble number density. The measured bubble number densities can be reconciled with model simulations if homogeneous nucleation energy is scaled with $\alpha \leq \alpha_{max}$. Only Pinatubo can be reconciled with homogeneous nucleation whereas all other eruptions require $\alpha < 1$. The red shaded area shows the range of α that can match observed bubble number densities in all eruptions. (b) Heterogeneous nucleation factor, α_{Het} versus contact angle, θ, for different minerals. Estimates are for magnetite [34, 35], for hematite [34, 36], and for feldspar [35]. Magnetite is the only mineral phase that allows heterogeneous nucleation to simultaneously match observed bubble number densities in all eruptions.

homogeneous nucleation did not match the observation, we established a maximum nucleation factor , α_{max}, such that the simulation can match the observed bubble density if W_n is reduced through scaling by $0 < \alpha \leq \alpha_{max}$. We find that 1991 Pinatubo (Philippines) is the only eruption where homogeneous nucleation ($\alpha_{max} = 1$) can result in the observed bubble number density. In all other eruptions W_n must be scaled by $\alpha < 1$ (Figure 2a). W_n can be reduced through different physical processes. The presence of solid heterogeneities, for instance, may reduce W_n by providing low surface energy sites for bubble nucleation [32]. During such heterogeneous nucleation, W_n is scaled by heterogeneous nucleation factor, $\alpha_{Het} \leq 1$. An alternative to reducing W_n are halogens. Gardner et al. [22] demonstrated that the presence of 1 wt% Fluorine scales W_n by $\alpha \approx \frac{1}{4}$. The amount of Fluorine in most eruptions is, however, in the order of 200-1500 ppm [2]. In what follows we thus only focus on heterogeneous nucleation.

Heterogeneous nucleation in magmatic systems is facilitated by the presence of crystalline molecular aggregates which provide nucleation sites for bubbles. The value of α_{Het} depends on the contact angle, θ, between the melt-bubble interface and the pre-existing crystal (Figure 2b). Direct measurements of θ for bubble nuclei is impossible because they are too small and ephemeral. Some studies have attempted to estimate θ from contact between microscopically observed bubbles and crystals [35]. It is, however, unlikely that the contact angle is the same for nuclei and microscapically observable bubbles because the thermodynamic properties are different for bubble nuclei and microscopic bubbles [25, 32]. Instead, θ has been inferred from the difference in pressure at which bubbles first nucleate during decompression in homogeneous and heterogeneous nucleation experiments with $\alpha_{Het} = (\Delta P_{Het}/\Delta P_{Hom})^2$ [32, 34]. Based on such experiments, it has been shown that the contact angle is dependent on the substrate's mineralogical structure (Figure 2b). For example, the contact angle for feldspar is approximately 20° [35], whereas for hematite it is approximately 90°-100° [36, 34], and for magnetite it is approximately 145°-160° [35, 34]. Magnetite is thus the most efficient mineral phase in facilitating bubble nucleation. A comparison between α_{max} and α_{het} in Figure 2 illustrates that magnetite is the only mineral phase that can simultaneously match observed bubble number densities in all seven eruptions.

3 RECONSTRUCTING ERUPTION DYNAMICS

For each eruption we ran simulations wherein W_n is scaled with α_{Het} spanning the range associated with contact angles for magnetite. For each value of θ we determined the average decompression rate at which the magma would be predicted to fragment at a bubble number density equal to the observed value. The resultant average decompression rates range between 0.1 MPa/s and 1 MPa/s (Figure 3). Decompression rates are correlated with magma ascent rate, which varies between 10 m/s to 100 m/s at fragmentation. Our decompression rate estimates are substantially lower than conventional estimates based on homogeneous nucleation and are consistent with independent estimates from melt embayments [37], and from conduit models [38, 39]. Decompression rate estimates from ground mass crystallization and from crystals rims tend to be low [40, 41, 20], and it has been suggested that these techniques may provide a potential lower bound on decompression rates of fast ascending explosive eruptions rather than being representative of a defined estimate [42].

Heterogeneous nucleation exerts a complex feedback between water exsolution, decompression rate, and explosive fragmentation. Figure 4 provides a representative example of such feedback for $\theta = 145°$. Heterogeneous nucleation energy is low enough that nucleation peaks at supersaturation pressures of 15

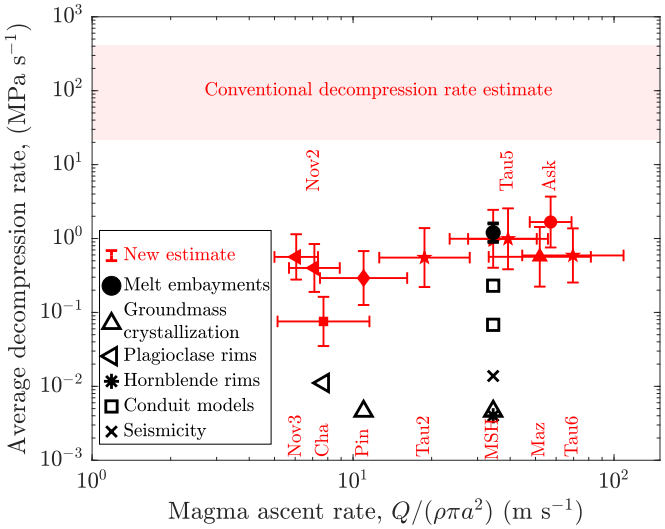

Figure 3: Simulated decompression rates for heterogeneous nucleation on magnetite (red symbols). The vertical errorbars show the range of calculated decompression rates and the horizontal errorbars represent the corresponding range of magma ascent rate; both as a result of the uncertainty in magnetite contact angle. Decompression rate estimates are correlated with magma ascent rate estimated from $Q/\rho_m \pi a^2$, where Q is mass discharge rate, ρ_m is magma density, a is the conduit radius, and ϕ is the volume fraction of bubbles at fragmentation. Results are consistent with independent estimates from diffusion profiles in melt embayments [37] and conduit models [38, 39]. Other estimates shown are based on seismisity [43], , plagioclase rims [13], hornblende rims [41, 20], and groundmass crystallization [40].

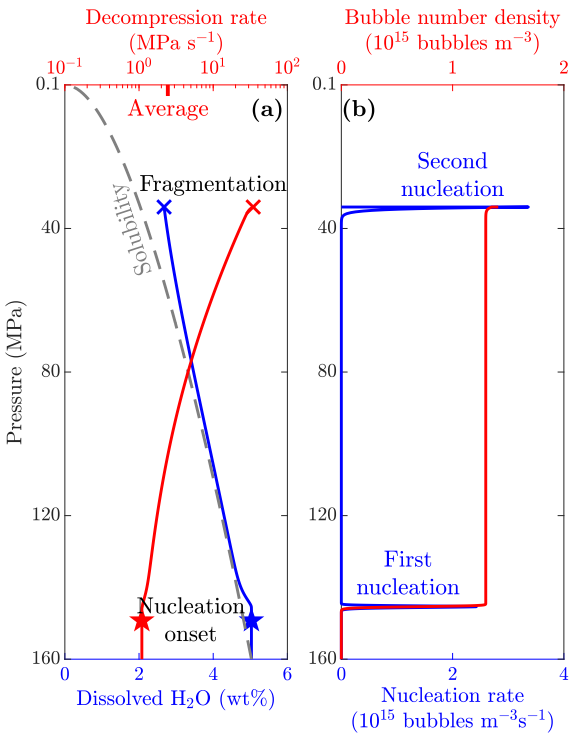

Figure 4: Illustrative model results of the feedback between water exsolution, decompression rate, and magma fragmentation for heterogeneous nucleation with $\theta = 145°$. Nucleation first occurs at low supersaturation. Subsequently H_2O concentration remains close to equilibrium because of diffusion of H_2O molecules into nucleated bubbles. This results in a progressive increase in viscosity and, hence, decompression rate. Subsequently, supersaturation pressure increases gradually which leads to a second nucleation event, followed by magma fragmentation.

MPa. After nucleation, H_2O diffuses into existing bubbles as magma continues to decompress. The nucleated bubbles from the first nucleation event result in a sufficiently small characteristic diffusion length such that H_2O can efficiently diffuse into the existing bubbles as the magma continues to decompress. Consequently, the average dissolved H_2O concentration remains close to equilibrium. As a result of H_2O exsolution viscosity and consequently the decompression rate increase. At the same time supersaturation increases gradually. Eventually this results in a second nucleation peak with a higher rate than the first one. Because of the substantial overpressure in the newly nucleated bubbles, fragmentation conditions are reached immediately after the second nucleation peak.

Our simulation results suggest that the discrepancies between homogeneous nucleation experiments and observed bubble number densities in Plinian silicic eruptions can be resolved by heterogeneous nucleation in the presence of magnetite. Our findings are in agreement with the heterogeneous nucleation hypothesis by Shea [44]. For none of the eruptions studied here, however, magnetite crystals have been reported at number densities similar to or greater than bubble number density. Tephra samples for which bubble number density have been measured were analyzed using scanning electron microscopy at a resolution down to approximately 1 micron. Magnetite in the range of 1-100 nm in size have, however, been documented within the glassy groundmass of pyroclasts from several explosive eruptions. For example, Schlinger et al. [45] reported magnetite nanolites as small as 20 nm in samples from Paintbrush Tuff (USA), whereas Di Genova et al. [46, 47] documented magnetite nanolites in samples from Green Tuff (Italy) and Yellowstone (USA) using Raman spectroscopy. Mujin et al. [48] observed magnetite nanolites in samples from Shinmoedake Volcano, Japan, with sizes down to 1 nm and number densities of up to $\sim 10^{23}$ m^{-3} using transmission electron microscopy. Moreover, several experimental studies produced heterogeneous nucleation without detecting crystals, suggesting magnetite were present at the nano scale [35, 49]. These observations and experiments suggest that magnetite may present at nano-sclaes and provide an impetus for future investigation into the existence of nanolites within Plinian silicic samples.

Our analysis has been based on the hypothesis that heterogeneous nucleation sites exist at the nano-scale. Although nanolites probably form by rapid undercolling during water exsolution [48], to avoid assumptions about poorly constrained crystal nucleation rates [50], we did not attempt to simulate concurrent nanolite formation and bubble nucleation. Instead we assumed

nanolites are present prior to magma decompression. Our simulation results, however, serve to illustrate the possibility of syn-eruptive water exsolution and nanolites formation. Prior to an eruption magma is thought to contain exsolved gas phases of predominantly H_2O, CO_2 and SO_2 [2]. Upon decompression H_2O may exsolve into these pre-existing bubbles without further bubble nucleation. This may result in sufficient undercooling for formation of magnetite nanolites [48], ultimately leading to a shallow nucleation event near fragmentation.

In summary, we find that bubbles at number densities observed in pyroclastic samples from a wide range of Plinian silicic eruptions are consistent with heterogeneous nucleation on magnetite nanolites, if they are present at number densities similar to those discovered recently in explosively erupted pyroclasts. Such heterogeneous bubble nucleation can resolve the discrepancy between the inferred water saturation for many eruptions and that required to nucleate bubbles homogeneously. Heterogeneous nucleation would also resolve the long-standing controversy about the unrealistically high decompression rates required for homogeneous nucleation, relative to values predicted by melt embayments and conduit models. We thus conclude that heterogeneous bubble nucleation during Plinian silicic eruptions, facilitated by magnetite nanolites, is a viable hypothesis that provides impetus for future investigations, in particular a systematic search for the presence of magnetite nanolites in pyroclasts from Plinian silicic eruptions.

METHODS

3.1 Bubble nucleation

We used Classical Nucleation Theory to estimate nucleation rate of critical bubble nuclei at a given supersaturation pressure. Clusters of volatiles molecules that are larger than the critical nucleus size are stable and will grow into bubbles. The critical size, R_c, is given by [32]

$$R_c = \frac{2\gamma}{P_n - P_m}, \tag{1}$$

where γ is surface tension of bubble nuclei, P_n is pressure inside a bubble nucleus, and P_m is pressure in the surrounding melt. P_n is related to the saturation pressure of volatiles, P_{sat}, through [36]

$$f(P_n, T)P_n = f(P_{sat}, T)P_{sat}e^{\Omega(P_m - P_{sat})/k_B T}, \tag{2}$$

where T is temperature, $f(P, T)$ is the fugacity coefficient of the supersaturated volatile phase, Ω is the volume of volatile molecules, and k_B is the Boltzman constant.

The nucleation energy, W_n, is given by

$$W_n = \frac{16\pi\gamma^3}{3(P_n - P_m)^2}, \tag{3}$$

and the nucleation rate is

$$J = J_0 \exp\left(-\frac{W_n}{k_B T}\alpha\right), \tag{4}$$

with

$$J_0 = \frac{2\Omega n_0^2 D}{a_0}\sqrt{\frac{\gamma}{k_B T}}. \tag{5}$$

n_0 is the concentration of volatiles molecules in melt, D is the diffusion coefficient, a_0 is the average distance between volatiles molecules. and α is nucleation factor. Here we use heterogeneous nucleation factor, $\alpha = \alpha_{Het}$, which depends on the contact angle, θ, between bubble nuclei and crystals as

$$\alpha_{Het} = \frac{(2 - \cos\theta)(1 + \cos\theta)^2}{4}. \tag{6}$$

The nucleation rate is strongly controlled by surface tension, γ, such that a few percent variations in γ can change J by >10 orders of magnitude [28]. A reliable prediction of nucleation rate and consequently bubble number density thus requires a solid constraint on surface tension. Here we use the surface tension formulation defined by Hajimirza et al. [25] which has been shown to be able to predict observed bubble number density in homogeneous nucleation experiments reliably. γ is given by

$$\gamma = \frac{0.49\ \gamma_B}{1 + 2\delta/R_c}, \tag{7}$$

where γ_B is the surface tension measurements for macroscopic bubbles [51], and $\delta \approx 0.32$ nm is the Tolman length for bubble nuclei in rhyolite [25, 52].

3.2 Bubble growth

When a bubble nucleus forms the H_2O concentration at the bubble melt interface is determined by the solubility of H_2O of the pressure inside the bubble. This concentration is lower than the concentration in the surrounding water. The concentration gradient drives diffusion of H_2O molecules toward bubble nuclei. The resultant mass flux of H_2O into a bubble, q, is approximated using the mean-field approximation [33],

$$q = D\left(\frac{C_m - C_R}{R}\right), \tag{8}$$

where C_m and C_R are the average H_2O concentrations in the melt and at the bubble-melt interface, respectively. The mass of H_2O inside the bubble, m_b, will increase at the rate

$$\frac{dm_b}{dt} = 4\pi R^2 \rho_m q, \tag{9}$$

and the bubble will grow in size at a rate

$$\frac{dR}{dt} = \frac{R}{4\mu}\left(P_b - P_m - \frac{2\gamma}{R}\right). \tag{10}$$

Here μ is viscosity of melt surrounding the bubble, and P_b is pressure inside the bubble, estimated using the equation of state of H_2O. Inertial terms in equation 10 are neglected given that they are considerably lower than the viscous terms [33]

The above equations describe growth rate of a single bubble. Because the number of bubbles in the magma are too high to track growth rates for each bubble individually, we use the method of moments, which calculates the moments of distributions, defined as [33]

$$M_k(t) = \int_0^\infty R^k F(R, t)\, dR, \tag{11}$$

with the subscript k determining the order of the moment. Each moment refers to a measurable characteristic quantity [33]: M_0 is bubble number density, M_1/M_0 is mean bubble radius, and $M_3/(M_3 + 3/(4\pi))$ is the volume fraction of bubbles. The evolution of the zeroth moment through time is given by

$$\frac{dM_0}{dt} = J, \tag{12}$$

and the evolution of the higher order moments are

$$\frac{dM_k}{dt} = k\frac{dR}{dt}M_{k-1} + \frac{dM_0}{dt}R_c^k, \tag{13}$$

where k ≥ 1 and dR/dt is given by equation 10.

The concentration of H_2O dissolved within the melt decreases as a result of the diffusion of water into bubbles. Based on the conservation

of water molecules in magma, the rate of change in the concentration of dissolved H_2O is given by

$$\frac{dC_m}{dt} = -\frac{1}{\rho_m}\left(M_0\frac{dm_b}{dt} + \frac{dM_0}{dt}m_c\right), \quad (14)$$

where ρ_m is the melt density, assumed to be constant throughout magma decompression.

3.3 Decompression

The decompression rate of erupting magma is not constant, but depends on a complex feedback between water exsolution and viscous resisting forces [3, 53]. To avoid poorly constrained parameters associated with more sophisticated conduit models [54, 53], but retain the inherent dependency between decompression rate and H_2O exsolution [55, 56], pressure in the surrounding melt was calculated using the Darcy-Weisbach relation for flow in a cylindrical conduit of constant diameter [3]. We only simulate nucleation up to fragmentation because at fragmentation the decompression rate becomes small and the nucleation rate becomes negligible [53]. Decompression rate below fragmentation is estimated from the equation of motion for two phase flow, with variables averaged over the cross-sectional area of the conduit [3]. Conservations of mass and momentum are given by

$$\frac{d(\rho UA)}{dz} = 0, \quad (15)$$

and

$$\frac{dP_m}{dt} = -U\left(\rho U\frac{dU}{dz} + \rho g + F_{fric}\right), \quad (16)$$

respectively. Here ρ is magma density, averaged over melt and gas phases,

$$\rho = \phi\rho_g + (1-\phi)\rho_m. \quad (17)$$

ϕ is the volume fraction of bubbles, ρ_g and ρ_m are gas and melt densities respectively, U is magma ascent rate, g is gravitational acceleration, A is the cross sectional area of conduit, and F_{fric} is the friction force. The latter is calculated from the Darcy-Weisbach relation, $F = f\rho U^2/a$, where $f = 16/\mathrm{Re} = (8\mu)/(\rho Ua)$ is friction factor. a is the conduit radius, and μ is the magma viscosity, given by $\mu_m(1-\phi_{crystal}/0.6)^{(-5/2)}$. Here μ_m is the melt viscosity and $\phi_{crystal}$ is the volume fraction of crystals. Substituting equation 15 into equation 16, and replacing U with $Q/(\rho\pi a^2)$ gives decompression rate as

$$\frac{dP_m}{dt} = -\frac{Q}{\rho\pi a^2}\left(\rho g + \frac{Q}{\rho\pi a^2}\left(\frac{8\mu}{a^2} - \frac{d\rho}{dt}\right)\right), \quad (18)$$

where Q is the mass discharge rate.

3.4 Model simulation

We integrated equations 12, 13, 14, and 18 using the `ode15s` function of MATLAB®. For each eruption simulations initiate from the known saturation pressure, and with additional initial conditions

$$M_k = 0, \quad P_m = P_{H_2O} \quad \text{and} \quad C_m = C_{H_2O}, \quad (19)$$

where C_{H_2O} is a function of P_{H_2O} [57]. A given simulation ends when the fragmentation criterion of Spieler et al. [58] is recorded.

The objective of our model simulation is to estimate decompression rate. The observational constraints are observed bubble number density and the magma fragmentation condition must reach. All parameters in the governing system of equations are either specified or calculated from existing formulations: H_2O solubility [57], diffusion coefficient [59], equation of state [60], fugacity coefficient [60], surface tension [25], melt viscosity [61], and the molecular volume of H_2O [62]. Conduit radius, which is related to decompression rate through equation 18, is the only parameter that is not constraint. For each eruption the model simulations predict a conduit radius and subsequently decompression rate conditional to the observational constraints.

3.5 Maximum heterogeneous factor

To estimate the maximum heterogeneous factor, α_{max}, that allows model simulations to match the observed bubble number density for a given eruption, we simulated bubble nucleation under an instantaneous decompression from saturation pressure to atmospheric pressure. If homogeneous nucleation can match or exceed the observed bubble number density, then $\alpha_{max} = 1$. If not, we determined maximum value of α at which the observed bubble number density can be reached. An empirical fit to the α_{max} as a function of nucleation energy is calculated as

$$\alpha_{max} = \min\left\{\frac{(log_{10}(N_m) - k_1)}{k_2}\frac{k_B T}{W_n^*}, 1\right\}. \quad (20)$$

Here $k_1 = 26.5$ and $k_2 = 0.26$ are constants, N_m is the observed bubble number density, and W_n^* is the homogeneous nucleation energy for a supersaturation equal to H_2O saturation pressure. The empirical fit for N_m over the range of 10^{14} m^{-3} to 10^{16} m^{-3}, and for T=850°C is shown by the blue shaded region in Figure 2.

ACKNOWLEDGEMENTS

This material is based upon work supported by the National Science Foundation grants EAR-1348072 and EAR-1348050.

AUTHOR CONTRIBUTION

S.H. conducted the numerical simulation. All authors participated in interpretations of the results and preparation of the manuscript.

DATA AVAILABILITY

The data used are listed in the references. All equations in the numerical simulation are presented in the Methods.

REFERENCES

[1] S. Carey and H. Sigurdsson. The intensity of plinian eruptions. *Bulletin of Volcanology*, 51:28–40, 1989. doi: 10.1007/BF01086759.

[2] P. J. Wallace, T. Plank, M. Edmonds, and E. H. Hauri. Chapter 7 - volatiles in magmas. In H. Sigurdsson, B. Houghton, S. McNutt, R. Hazel, and J. Stix, editors, *The Encyclopedia of Volcanoes (Second Edition)*, pages 163 – 183. Academic Press, Amsterdam, 2015. doi: https://doi.org/10.1016/B978-0-12-385938-9.00007-9.

[3] L. Wilson, R. S. J. Sparks, and G. P. L. Walker. Explosive volcanic eruptions – IV. The control of magma properties and conduit geometry on eruption column behaviour. *Geophysical Journal International*, 63:117–148, 1980. doi: 10.1111/j.1365-246X.1980.tb02613.x.

[4] H. M. Gonnermann and M. Manga. Dynamics of magma ascent. In S. A. Fagents, T. K. P. Gregg, and M. C. Lopes, editors, *Modeling volcanic processes: The physics and mathematics of volcanism*, pages 55–84. Cambridge University Press, Cambridge, UK, 2013.

[5] M. Cassidy, M. Manga, K. V. Cashman, and O. Bachmann. Controls on explosive-effusive volcanic eruption styles. *Nature Communications*, 9, 2018. doi: 10.1038/s41467-018-05293-3.

[6] N. K. Adams, B. F. Houghton, and W. Hildreth. Abrupt transitions during sustained explosive eruptions: examples from the 1912 eruption of Novarupta, Alaska. *Bulletin of Volcanology*, 69:189–206, 2006. doi: 10.1007/s00445-006-0067-4.

[7] F. Alfano, C. Bonadonna, and L. Gurioli. Insights into eruption dynamics from textural analysis: the case of the May, 2008, Chaitén eruption. *Bulletin of Volcanology*, 74: 2095–2108, 2012. doi: 10.1007/s00445-012-0648-3.

[8] R. J. Carey, B. F. Houghton, and T. Thordarson. Abrupt shifts between wet and dry phases of the 1875 eruption of Askja Volcano: Microscopic evidence for macroscopic dynamics. *Journal of Volcanology and Geothermal Research*, 184:256–270, 2009. doi: 10.1016/j.jvolgeores.2009.04.003.

[9] B. F. Houghton, R. J. Carey, K. V. Cashman, C. J. N. Wilson, B. J. Hobden, and J. E. Hammer. Diverse patterns of ascent, degassing, and eruption of rhyolite magma during the 1.8 ka Taupo eruption, New Zealand: Evidence from clast vesicularity. *Journal of Volcanology and Geothermal Research*, 195:31–47, 2010. doi: 10.1016/j.jvolgeores.2010.06.002.

[10] C. Klug, K. V. Cashman, and C. Bacon. Structure and physical characteristics of pumice from the climactic eruption of Mount Mazama (Crater Lake), Oregon. *Bulletin of Volcanology*, 64:486–501, 2002. doi: 10.1007/s00445-002-0230-5.

[11] H. S. Crosweller, B. Arora, S. K. Brown, E. Cottrell, N. I. Deligne, N. O. Guerrero, L. Hobbs, K. Kiyosugi, S. C. Loughlin, J. Lowndes, M. Nayembil, L. Siebert, R. S. J. Sparks, S. Takarada, and E. Venzke. Global database on large magnitude explosive volcanic eruptions (LaMEVE). *Journal of Applied Volcanology*, 1:1–13, 2012. doi: 10.1186/2191-5040-1-4.

[12] H. Sigurdsson and R. S. J. Sparks. Petrology of Rhyolitic and Mixed Magma Ejecta from the 1875 Eruption of Askja, Iceland. *Journal of Petrology*, 22:41–84, 1981. doi: 10.1093/petrology/22.1.41.

[13] J. M. Castro and D. B. Dingwell. Rapid ascent of rhyolitic magma at Chaitén Volcano, Chile. *Nature*, 461:780–783, 2009. doi: 10.1038/nature08458.

[14] C. R. Bacon and T. H. Druitt. Compositional evolution of the zoned calcalkaline magma chamber of Mount Mazama, Crater Lake, Oregon. *Contributions to Mineralogy and Petrology*, 98:224–256, 1988. doi: 10.1007/BF00402114.

[15] S. Carey, H. Sigurdsson, J. E. Gardner, and W. Cristwell. Variations in column height and chamber during the May 18, 1980 eruption of Mt. St. Helens. *Journal of Volcanology and Geothermal Research*, 43:99–112, 1990. doi: 10.1016/0377-0273(90)90047-J.

[16] M. J. Rutherford, H. Sigurdsson, S. Carey, and A. Davis. The May 18, 1980, eruption of Mount St. Helens. 1. Melt composition and experimental phase equilibria. *Journal of Geophysical Research*, 90:2929–2947, 1985. doi: 10.1029/JB090iB04p02929.

[17] C. Klug and K. V. Cashman. Vesiculation of May 18, 1980, Mount St. Helens magma. *Geology*, 22:468, 1994. doi: 10.1130/0091-7613(1994)022<0468:VOMMSH>2.3.CO;2.

[18] J. E. Hammer, M. J. Rutherford, and W. Hildreth. Magma storage prior to the 1912 eruption at Novarupta, Alaska. *Contributions to Mineralogy and Petrology*, 144:144–162, 2002. doi: 10.1007/s00410-002-0393-2.

[19] M. Polacci, P. Papale, and M. Rosi. Textural heterogeneities in pumices from the climactic eruption of Mount Pinatubo, 15 June 1991, and implications for magma ascent dynamics. *Bulletin of Volcanology*, 63:83–97, 2001. doi: 10.1007/s004450000123.

[20] J. E. Hammer and M. J. Rutherford. An experimental study of the kinetics of decompression-induced crystallization in silicic melt. *Journal of Geophysical Research: Solid Earth*, 107:ECV 8–1–ECV 8–24, 2002. doi: 10.1029/2001jb000281.

[21] J. E. Gardner and R. A. Ketcham. Bubble nucleation in rhyolite and dacite melts: Temperature dependence of surface tension. *Contributions to Mineralogy and Petrology*, 162:929–943, 2011. doi: 10.1007/s00410-011-0632-5.

[22] J. E. Gardner, S. Hajimirza, J. D. Webster, and H. M. Gonnermann. The impact of dissolved fluorine on bubble nucleation in hydrous rhyolite melts. *Geochimica et Cosmochimica Acta*, 226:174–181, 2018. doi: 10.1016/j.gca.2018.02.013.

[23] H. M. Gonnermann and J. E. Gardner. Homogeneous bubble nucleation in rhyolitic melt: Experiments and nonclassical theory. *Geochemistry, Geophysics, Geosystems*, 14(11):4758–4773, 2013. doi: 10.1002/ggge.20281.

[24] T. Giachetti, H. M. Gonnermann, J. E. Gardner, A. Burgisser, S. Hajimirza, T. C. Earley, N. Truong, and P. Toledo. Bubble Coalescence and Percolation Threshold in Expanding Rhyolitic Magma. *Geochemistry, Geophysics, Geosystems*, 20:1054–1074, 2019. doi: 10.1029/2018GC008006.

[25] S. Hajimirza, H. M. Gonnermann, J. E. Gardner, and T. Giachetti. Predicting homogeneous bubble nucleation in rhyolite. *Journal of Geophysical Research: Solid Earth*, 124:2395–2416, 2019. doi: 10.1029/2018JB015891.

[26] M. Hamada, D. Laporte, N. Cluzel, K. T. Koga, and T. Kawamoto. Simulating bubble number density of rhyolitic pumices from Plinian eruptions: constraints from fast decompression experiments. *Bulletin of Volcanology*, 72:735–746, 2010. doi: 10.1007/s00445-010-0353-z.

[27] M. T. Mangan and T. Sisson. Delayed, disequilibrium degassing in rhyolite magma: decompression experiments and implications for explosive volcanism. *Earth and Planetary Science Letters*, 183:441–455, 2000. doi: 10.1016/S0012-821X(00)00299-5.

[28] M. T. Mangan and T. Sisson. Evolution of melt-vapor surface tension in silicic volcanic systems: Experiments with hydrous melts. *Journal of Geophysical Research*, 110: B01202, 2005. doi: 10.1029/2004JB003215.

[29] C. C. Mourtada-Bonnefoi and D. Laporte. Homogeneous bubble nucleation in rhyolitic magmas: An experimental study of the effect of H2O and CO2. *Journal of Geophysical Research: Solid Earth*, 107(B4):ECV 2–1–ECV 2–19, 2002. doi: 10.1029/2001JB000290.

[30] C. C. Mourtada-Bonnefoi and D. Laporte. Kinetics of bubble nucleation in a rhyolitic melt: an experimental

study of the effect of ascent rate. *Earth and Planetary Science Letters*, 218(3-4):521–537, 2004. doi: 10.1016/S0012-821X(03)00684-8.

[31] A. Toramaru. BND (bubble number density) decompression rate meter for explosive volcanic eruptions. *Journal of Volcanology and Geothermal Research*, 154:303–316, 2006. doi: 10.1016/j.jvolgeores.2006.03.027.

[32] O. Navon and V. Lyakhovsky. Vesiculation processes in silicic magmas. In J. S. Gilbert and R. S. J. Sparks, editors, *The physics of explosive volcanic eruptions*, pages 27–50. Geological Society, London, Special Publications, Cambridge, UK, 1998.

[33] A. Toramaru. Numerical study of nucleation and growth of bubbles in viscous magmas. *Journal of Geophysical Research: Solid Earth*, 100:1913–1931, 1995. doi: 10.1029/94JB02775.

[34] J. E. Gardner and M. Denis. Heterogeneous bubble nucleation on Fe-Ti oxide crystals in high-silica rhyolitic melts. *Geochimica et Cosmochimica Acta*, 68:3587–3597, 2004. doi: 10.1016/j.gca.2004.02.021.

[35] S. Hurwitz and O. Navon. Bubble nucleation in rhyolitic melts: Experiments at high pressure, temperature, and water content. *Earth and Planetary Science Letters*, 122:267–280, 1994. doi: 10.1016/0012-821X(94)90001-9.

[36] N. Cluzel, D. Laporte, A. Provost, and I. Kannewischer. Kinetics of heterogeneous bubble nucleation in rhyolitic melts: implications for the number density of bubbles in volcanic conduits and for pumice textures. *Contributions to Mineralogy and Petrology*, 156:745–763, 2008. doi: 10.1007/s00410-008-0313-1.

[37] M. C. S. Humphreys, T. Menand, J. D. Blundy, and K. Klimm. Magma ascent rates in explosive eruptions: Constraints from H_2O diffusion in melt inclusions. *Earth and Planetary Science Letters*, 270:25–40, 2008.

[38] S. Carey and H. Sigurdsson. The May 18, 1980 eruption of Mount St. Helens: 2. Modeling of dynamics of the Plinian phase. *Journal of Geophysical Research*, 90:2948, 1985. doi: 10.1029/JB090iB04p02948.

[39] P. Papale and F. Dobran. Magma flow along the volcanic conduit during the Plinian and pyroclastic flow phases of the May 18, 1980, Mount St. Helens eruption. *Journal of Geophysical Research*, 99:4355–4373, 1994. doi: 10.1029/93JB02972.

[40] C. H. Geschwind and M. J. Rutherford. Crystallization of microlites during magma ascent: the fluid mechanics of 1980-1986 eruptions at Mount St. Helens. *Bulletin of Volcanology*, 57:356–370, 1995.

[41] M. J. Rutherford and P. M. Hill. Magma ascent rates from amphibole breakdown: An experimental study applied to the 1980-1986 Mount St. Helens Eruptions. *Journal of Geophysical Research: Solid Earth*, 98:19667–19685, 1993. doi: 10.1029/93JB01613.

[42] M. J. Rutherford. Magma Ascent Rates. *Reviews in Mineralogy and Geochemistry*, 69:241–271, 2008. doi: 10.2138/rmg.2008.69.7.

[43] R. Scandone and S. D. Malone. Magma supply, magma discharge and readjustment of the feeding system of mount St. Helens during 1980. *Journal of Volcanology and Geothermal Research*, 23:239–262, 1985. doi: 10.1016/0377-0273(85)90036-8.

[44] T. Shea. Bubble nucleation in magmas: A dominantly heterogeneous process? *Journal of Volcanology and Geothermal Research*, 343:155–170, 2017. doi: 10.1016/j.jvolgeores.2017.06.025.

[45] C. M. Schlinger, J. G. Rosenbaum, and D. R. Veblen. Fe-oxide microcrystals in welded tuff from southern Nevada: Origin of remanence carriers by precipitation in volcanic glass. *Geology*, 16:556–559, 1988. doi: 10.1130/0091-7613(1988)016<0556:FOMIWT>2.3.CO;2.

[46] D. Di Genova, S. Kolzenburg, S. Wiesmaier, E. Dallanave, D. R. Neuville, K. U. Hess, and D. B. Dingwell. A compositional tipping point governing the mobilization and eruption style of rhyolitic magma. *Nature*, 552:235–238, 2017. doi: 10.1038/nature24488.

[47] D. Di Genova, A. Caracciolo, and S. Kolzenburg. Measuring the degree of "nanotilization" of volcanic glasses: Understanding syn-eruptive processes recorded in melt inclusions. *Lithos*, 318-319:209–218, 2018. doi: 10.1016/j.lithos.2018.08.011.

[48] M. Mujin, M. Nakamura, and A. Miyake. Eruption style and crystal size distributions: Crystallization of groundmass nanolites in the 2011 Shinmoedake eruption. *American Mineralogist*, 102:2367–2380, 2017. doi: 10.2138/am-2017-6052CCBYNCND.

[49] J. E. Gardner, M. Hilton, and M. R. Carroll. Experimental constraints on degassing of magma: isothermal bubble growth during continuous decompression from high pressure. *Earth and Planetary Science Letters*, 168:201–218, 1999. doi: 10.1016/S0012-821X(99)00051-5.

[50] P. G. Vekilov. Crystallization tracked atom by atom. *Nature*, 570(7762):450–452, 2019. doi: 10.1038/d41586-019-01965-2.

[51] N. Bagdassarov, A. Dorfman, and D. B. Dingwell. Effect of alkalis, phosphorus, and water on the surface tension of haplogranite melt. *American Mineralogist*, 85:33–40, 2000. doi: 10.2138/am-2000-0105.

[52] R. C. Tolman. The Effect of Droplet Size on Surface Tension. *The Journal of Chemical Physics*, 17:333–337, 1949. doi: 10.1063/1.1747247.

[53] H. Massol and T. Koyaguchi. The effect of magma flow on nucleation of gas bubbles in a volcanic conduit. *Journal of Volcanology and Geothermal Research*, 143:69–88, 2005. doi: 10.1016/j.jvolgeores.2004.09.011.

[54] S. Colucci, M. M. Vitturi, A. Neri, and D. M. Palladino. An integrated model of magma chamber, conduit and column for the analysis of sustained explosive eruptions. *Earth and Planetary Science Letters*, 404:98–110, 2014. doi: 10.1016/j.epsl.2014.07.034.

[55] H. M. Gonnermann and M. Manga. Nonequilibrium magma degassing: Results from modeling of the ca. 1340 A.D. eruption of Mono Craters, California. *Earth and Planetary Science Letters*, 238:1–16, 2005. doi: 10.1016/j.epsl.2005.07.021.

[56] H. M. Gonnermann and M. Manga. The fluid mechanics inside a volcano. *Annual Review of Fluid Mechanics*, 39: 321–356, 2007. doi: 10.1146/annurev.fluid.39.050905.110207.

[57] Y. Liu, Y. Zhang, and H. Behrens. Solubility of H_2O in rhyolitic melts at low pressures and a new empirical model for mixed H_2O–CO_2 solubility in rhyolitic melts. *Journal of Volcanology and Geothermal Research*, 143:219–235, 2005. doi: https://doi.org/10.1016/j.jvolgeores.2004.09.019.

[58] O. Spieler, B. Kennedy, U. Kueppers, D. B. Dingwell, B. Scheu, and J. Taddeucci. The fragmentation threshold of pyroclastic rocks. *Earth and Planetary Science Letters*, 226:139–148, 2004. doi: 10.1016/j.epsl.2004.07.016.

[59] Y. Zhang and H. Behrens. H_2O diffusion in rhyolitic melts and glasses. *Chemical Geology*, 169:243–262, 2000. doi: https://doi.org/10.1016/s0009-2541(99)00231-4.

[60] J. R. Holloway. *Fugacity and activity of molecular species in supercritical fluids*. Springer Netherlands, Dordrecht, Netherlands, 1977. doi: https://doi.org/10.1007/978-94-010-1252-2_9.

[61] H. Hui and Y. Zhang. Toward a general viscosity equation for natural anhydrous and hydrous silicate melts. *Geochimica et Cosmochimica Acta*, 71:403–416, 2007. doi: https://doi.org/10.1016/j.gca.2006.09.003.

[62] F. A. Ochs and R. A. Lange. The density of hydrous magmatic liquids. *Science*, 283:1314–1317, 1999. doi: https://doi.org/10.1126/science.283.5406.1314.